Stratospheric heating by potential geoengineering aerosols

A. J. Ferraro,[1] E. J. Highwood,[1] and A. J. Charlton-Perez[1]

Received 23 September 2011; revised 15 November 2011; accepted 19 November 2011; published 28 December 2011.

[1] A fixed dynamical heating model is used to investigate the pattern of zonal-mean stratospheric temperature change resulting from geoengineering with aerosols composed of sulfate, titania, limestone and soot. Aerosol always heats the tropical lower stratosphere, but at the poles the response can be either heating, cooling, or neutral. The sign of the change in stratospheric Pole-Equator temperature difference depends on aerosol type, size and season. This has implications for modeling geoengineering impacts and the response of the stratospheric circulation. **Citation:** Ferraro, A. J., E. J. Highwood, and A. J. Charlton-Perez (2011), Stratospheric heating by potential geoengineering aerosols, *Geophys. Res. Lett.*, *38*, L24706, doi:10.1029/2011GL049761.

1. Introduction

[2] Geoengineering is defined by *Shepherd et al.* [2009] as "deliberate large-scale intervention in the Earth's climate system in order to moderate global warming". As Earth's climate has warmed and efforts to slow the rate of increase in anthropogenic greenhouse gas emissions have failed, geoengineering has been proposed as an alternative way to mitigate the warming. *Crutzen* [2006] encouraged research on geoengineering by injection of aerosol particles into the stratosphere to increase the planetary albedo. We refer to this technique as 'stratospheric SRM (Solar Radiation Management)'.

[3] *Rasch et al.* [2008] reviewed the state of the science of stratospheric SRM. Using a climate model they showed that stratospheric SRM using sulfate would result in global-mean surface cooling with substantial spatial variation. Precipitation patterns are also expected to change, including a decrease in total global precipitation [*Robock et al.*, 2008]. Geoengineering aerosols could also alter the dynamics of the stratosphere by changing radiative heating rates. For example, *Tilmes et al.* [2009] show an intensified polar vortex in their SRM simulations, which results in a stronger, longer-lived, winter polar transport barrier.

[4] *Braesicke et al.* [2010] show that reducing solar irradiance in a chemistry-climate model changes El Nino Southern Oscillation teleconnections to the North Pole region, by changing ozone concentrations and the propagation of planetary waves. However, reducing the total solar irradiance is an unrealistic way to simulate stratospheric SRM because it does not represent aerosol heating and cooling in the stratosphere.

[5] Much research to date has considered the enhanced sulfate layer produced by volcanic sulfur dioxide emission to be an appropriate natural analogue [e.g., *Robock et al.*, 2008]. *Ramachandran et al.* [2000] quantified the radiative heating rates in the lower stratosphere following the eruption of Mt. Pinatubo. Such a change in stratospheric temperature would be expected to affect stratospheric dynamics. Indeed, *Stenchikov et al.* [2002] showed that the eruption produced a warm anomaly in winter in Northern Europe, consistent with an anomalously positive phase of the Arctic Oscillation. They showed this was due to a strengthened meridional temperature gradient in the lower stratosphere, amplified by ozone depletion and decreased planetary wave activity. Such feedbacks could also occur as a result of heating due to stratospheric SRM. *Gerber et al.* [2010] review modeled interactions between the polar vortex and tropospheric annular-mode patterns.

[6] The radiative impact of SRM in the stratosphere needs to be quantified before we can investigate potential dynamical changes. A major uncertainty in this impact is the aerosol size distribution. *Niemeier et al.* [2010] showed that the size distribution affects the amount of cooling at the surface and the stratospheric radiative heating. The aerosol composition is also important. Aerosols such as soot [*Blackstock et al.*, 2009], limestone dust [*Fujii*, 2011] and titanium dioxide [*Pope et al.*, 2011] could also be used.

[7] In this paper we investigate the stratospheric temperature change for a range of geoengineering aerosol species and size distributions. This is a preliminary step in understanding the importance of the stratospheric dynamics to the impacts of stratospheric SRM.

2. Method

2.1. Model

[8] We use *Edwards and Slingo*'s [1996] two-stream radiative transfer code (henceforth ES) to calculate radiative fluxes and heating rates when an aerosol layer is added to the stratosphere. The code is driven by the climatology from a 20-year integration of the HadGAM1 climate model. *Maycock et al.* [2011] provide a description of ES. Stratospheric temperature change is calculated using the fixed dynamical heating (FDH) approximation [*Fels et al.*, 1980]. Stratospheric temperatures are adjusted until the stratosphere converges to radiative equilibrium. FDH therefore approximates the temperature change with no dynamical feedback. This method separates the radiative impact from dynamical changes. The model does not include the radiative effects on the stratosphere of changing surface temperature. It therefore represents the response of the stratosphere on short timescales, before the surface temperature has changed.

2.2. Aerosol Layer Properties

[9] Aerosol residence time is maximized for injection at high altitudes. However, there are technological limits to the input altitude of geoengineering aerosols. *Robock et al.* [2009] claim that plastic balloons burst at approximately 25 km. *Heckendorn et al.* [2009] find that spreading sulfur

[1]Department of Meteorology, University of Reading, Reading, UK.

0094-8276/11/2011GL049761

Table 1. Parameters for Lognormal Size Distributions[a]

Aerosol	Mass (Tg)	R_{small} (μm)	R_{med} (μm)	R_{large} (μm)	σ_{narrow}	σ_{wide}	Notes
Sulfate	14.5	0.1	0.3	0.5	1.3	2.0	Refractive index: *World Meteorological Organization* (*WMO*) [1986]. Size: *Hommel and Graf* [2010]. Standard deviation: *Rasch et al.* [2008].
Titania	3	0.1	0.5	1.0	1.4	2.0	Refractive index: *Ribarsky* [1985]. Size: *Tegen and Lacis* [1996]. Standard deviation: WIDE [*Fujii*, 2011], NARROW [*Linke et al.*, 2006].
Limestone	18	0.1	0.5	1.0	1.4	2.0	As titania, except for refractive index: *Orofino et al.* [2002].
Soot	0.9	0.03	0.06	0.1	1.4	2.0	Refractive index: *WMO* [1986]. Size: *Rose et al.* [2006]. Standard deviation: *WMO* [1986] and *Pueschel* [1996].

[a]*R* denotes median radius, σ the geometric standard deviation.

dioxide emissions over a thicker layer decreases the size of the resulting aerosol by decreasing coagulation, which maximizes shortwave (SW) scattering. We spread the aerosol in a globally-uniform layer between the tropopause and 22 km. Our uniform, flat aerosol layer is an idealized setup. *Heckendorn et al.* [2009] show that in reality the aerosol layer would slope downwards towards the poles as a result of the sinking limb of the Brewer-Dobson circulation.

[10] We study aerosols composed of sulfuric acid (sulfate), titanium dioxide (titania), limestone dust and soot. We explore the uncertainty in the aerosol microphysics by considering six lognormal size distributions for each aerosol species, characterized by three median radii (SMALL, MEDIUM, LARGE) and two geometric standard deviations (NARROW, WIDE). The parameters for the size distributions, required for Mie calculations of absorption and scattering, are shown in Table 1. The absorption/scattering efficiencies of the SMALL/WIDE distributions are shown in Figure 1.

[11] The aerosol mass is chosen such that the SMALL/WIDE cases all have an instantaneous radiative forcing at the tropopause of -3.5 ± 0.1 Wm^{-2}. Since radiative properties are a function of aerosol size, the other distributions will produce a different radiative forcing. Instantaneous forcing is used to measure radiative impact rather than the

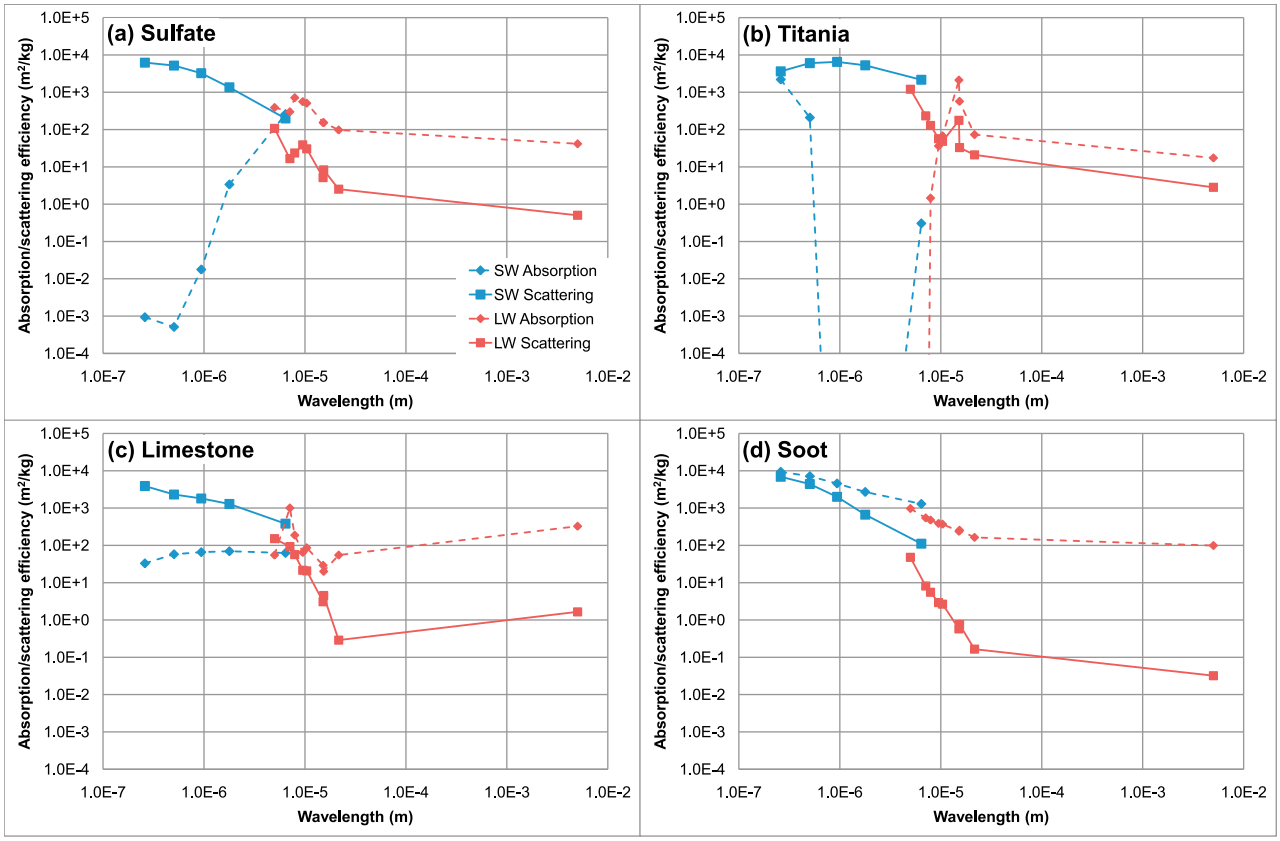

Figure 1. (a–d) Absorption/scattering efficiencies for the SMALL/WIDE aerosol size distributions. Points are plotted at the mid-point of each wavelength interval.

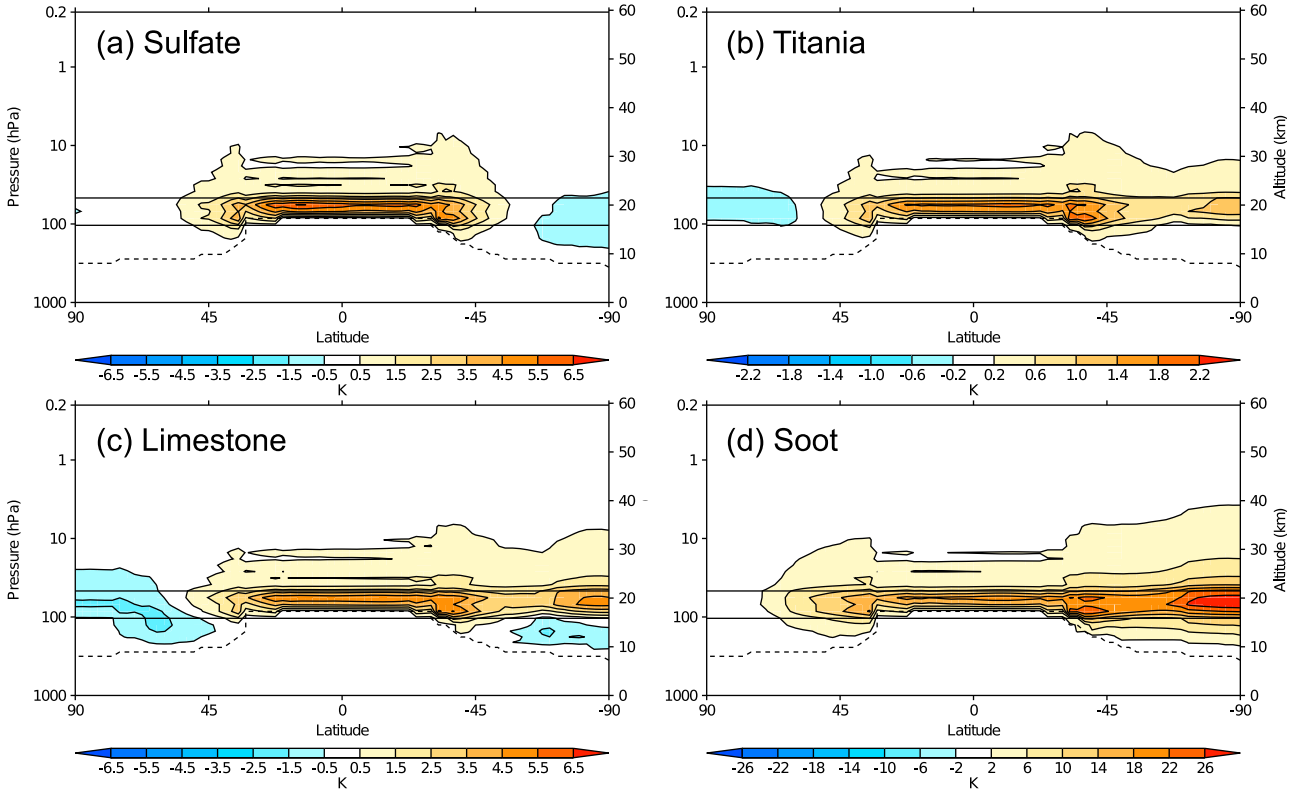

Figure 2. (a–d) Zonal-mean temperature change in DJF for the SMALL/WIDE aerosol size distributions. Note the different color scales. The tropopause is marked with a dashed line, the aerosol layer with solid black lines.

conventional definition of radiative forcing where the stratospheric temperatures are allowed to adjust. For most aerosol types the stratospheric adjustment has a negligible impact on the radiative forcing [*Hansen et al.*, 1997].

3. Results

[12] Figure 2 shows the result of the FDH stratospheric temperature adjustment for the SMALL/WIDE case in the December-January-February (DJF) season. The June-July-August (JJA) season shows a qualitatively similar pattern but with the poles reversed (not shown). We do not show the SON and MAM seasons because these seasons represent transitions between a warm and cold polar stratosphere. Figures 2a–2d produce the same instantaneous radiative forcing at the tropopause. The differences between the instantaneous and stratosphere-adjusted radiative forcings are less than 10% of the instantaneous value, with the exception of soot, where the forcing is 48% less than the instantaneous forcing. This is because strong heating in the stratosphere increases downward longwave (LW) emission to the surface.

[13] When interpreting these results it is useful to consider the energy balance of a layer in the lower stratosphere. The main input is from solar SW radiation. The stratosphere cools by emitting longwave radiation proportionally to its temperature. There is some upwelling LW radiation from the troposphere which is absorbed in the stratosphere, but this is generally smaller than the incoming SW. Temperature change due to aerosol will be principally governed by SW absorption and LW emission.

[14] Figure 2a shows the stratospheric temperature change for sulfate aerosol. It closely resembles the volcanic pattern, with heating in the tropical lower stratosphere and cooling over the summer pole. We see from Figure 1a that sulfate absorbs moderately in the LW part of the spectrum. Over the summer pole the stratosphere is relatively warm, so sulfate emits strongly in the LW and produces a radiative cooling. The tropical heating is a result of the flux convergence from absorption of LW radiation from the warm troposphere below and minimal emission from the cold tropical lower stratosphere.

[15] The temperature change from titania (Figure 2b) is approximately 30% of that from sulfate. There is heating at all latitudes except at the winter pole. This is because (as shown in Figure 1b) titania absorbs mainly in the shortest wavelengths. Hence there is heating in the latitudes receiving solar radiation. The North Pole is under polar night conditions in DJF, so there is no solar heating and LW cooling dominates.

[16] Limestone (Figures 1c and 2c) displays a very similar pattern to titania (of greater magnitude) but with cooling at lower levels over the South (summer) Pole. Extinction (by absorption and scattering) of incoming solar radiation reduces the radiation available for heating at lower levels. The cooling appears only at the pole because this region is below the aerosol layer (at 17 km) but still in the stratosphere. The FDH approximation only applies in the stratosphere so tropospheric temperature change is not calculated.

[17] Finally, soot aerosol (Figures 1d and 2d) has the strongest heating over the summer pole. Soot absorbs strongly in the SW part of the spectrum so its heating pattern is constrained by the latitudinal variation of solar radiation. The magnitude of the heating is much greater than the other aerosols (greater than 20 K in some regions).

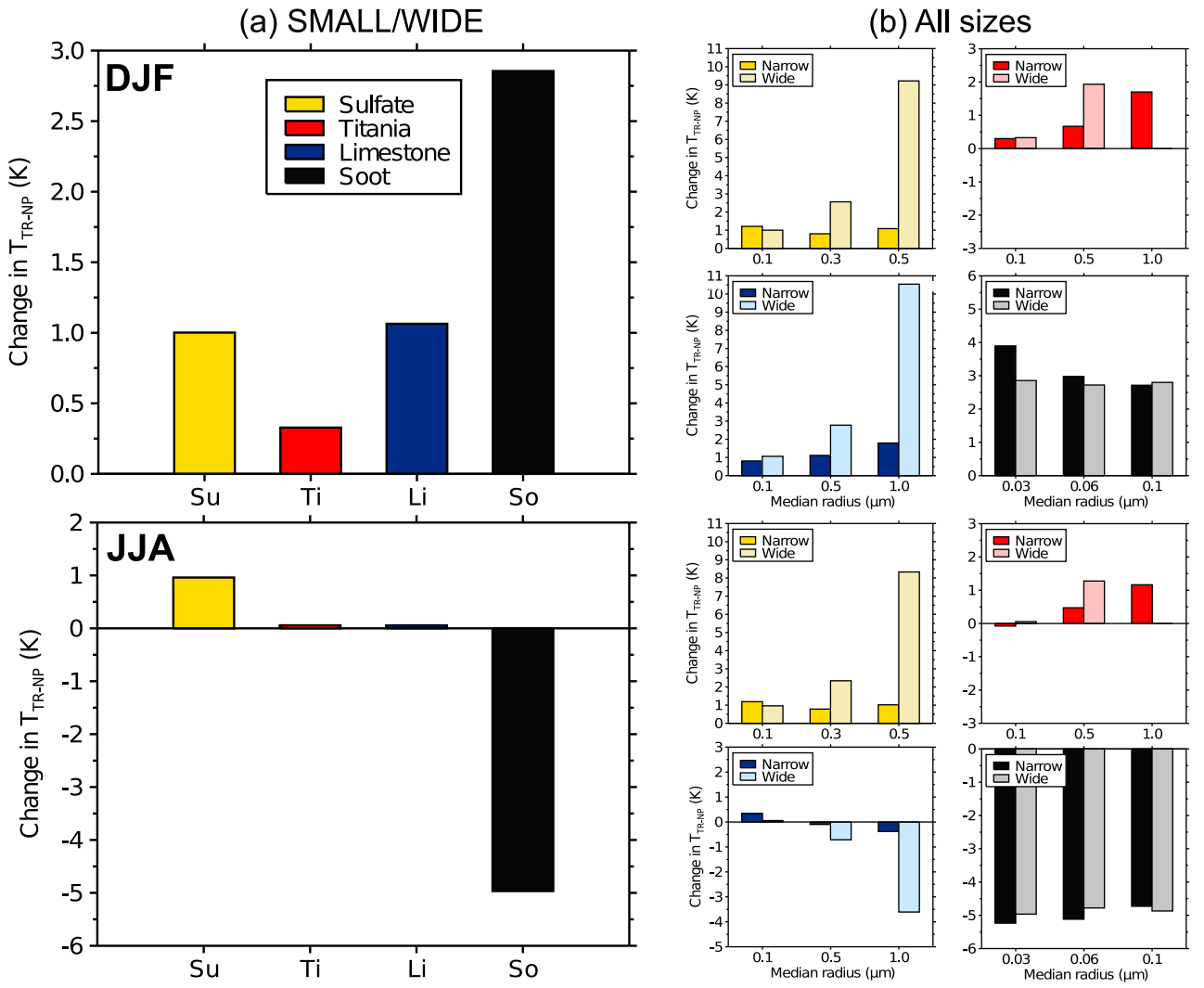

Figure 3. Change in lower stratospheric (17–22 km) temperature difference (K) between the Tropics (20N-20S) and the North Pole (90N-50N) per unit negative radiative forcing in DJF and JJA. (a) The SMALL/WIDE case (radiative forcing of -3.5 Wm^{-2}). (b) All size distributions.

[18] Aerosol always heats the tropical lower stratosphere, but at the poles the response can be either heating, cooling, or neutral. This affects the temperature contrast between the Pole and the Equator. We define $T_{TR-NP} = T_{TR} - T_{NP}$ as the difference in temperature between 20N-20S (Tropics) and 90N-50N (North Pole) per unit negative radiative forcing. This is calculated by dividing the temperature change from each model run by its instantaneous radiative forcing, assuming that the temperature response is a linear function of radiative forcing. We do not consider the Southern Hemisphere because the results show the same qualitative characteristics. Figure 3 shows the change in T_{TR-NP} for all aerosol distributions. A positive number represents cooling at the Pole and warming at the Equator. We do not show the LARGE/WIDE case for titania because the instantaneous radiative forcing is positive (0.04 Wm^{-2}) and hence of no use for SRM.

[19] In DJF the North Pole is characterized by a cold stratospheric vortex. All aerosol types and size distributions increase T_{TR-NP}. Figure 3a shows the change in T_{TR-NP} for the SMALL/WIDE case. In DJF titania produces the smallest change in temperature difference per unit negative radiative forcing (approximately 0.3 K). Sulfate and limestone both increase T_{TR-NP} by about 1 K, while soot has the largest impact at 2.8 K. In JJA the North Polar stratosphere is heated by additional SW absorption. Sulfate produces a very similar change in T_{TR-NP} in both seasons, titania and limestone have negligible impact and soot produces a strong negative change (-5 K).

[20] Figure 3b shows how the gradient changes with aerosol size distribution. Note that the lognormal size distribution parameters (median radius and geometric standard deviation) are different for each aerosol type. In the NARROW sulfate case there is little sensitivity to changing size. The WIDE case of soot is relatively insensitive to radius changes, and the smallest impact occurs for the LARGE radius. For all other cases in DJF increasing the radius and standard deviation increases T_{TR-NP} per unit negative radiative forcing. The effect is especially strong for the LARGE/WIDE sulfate and limestone cases where the aerosol mass is dominated by a few large particles which absorb in the LW.

[21] The bottom section of Figure 3b shows the JJA change in T_{TR-NP} depending on the size distribution. Titania increases the difference except in the SMALL/NARROW case. The LW absorption is small, so the pole does not cool by LW emission. Hence the pole in the SMALL/NARROW case is warmer than in the other titania cases. The sign of the change in T_{TR-NP} also changes with limestone. It is positive for the SMALL case and negative in the MEDIUM and LARGE cases. Once again, this is due to polar heating. Increasing the size and width of the limestone distribution increases the absorption of SW radiation. In JJA the summer pole is under constant sunlight, so a large amount of SW radiation is absorbed, heating the pole more than the tropics and reducing T_{TR-NP}. Soot produces very strong SW heating over the pole in all cases, decreasing T_{TR-NP}.

4. Discussion and Conclusions

[22] In this paper we have shown that four different stratospheric SRM aerosol species produce different patterns of stratospheric temperature change. Each panel in Figure 2 has the same instantaneous radiative forcing at the tropopause, which implies the same global cooling, but the atmospheric circulation response might be different in each case.

[23] The main drivers of the stratospheric temperature change due to aerosols are SW absorption and LW emission. Aerosols will also cool the surface and troposphere, reducing the upwelling LW radiation. Our model does not calculate tropospheric or surface temperature change, so this effect is not included. Surface temperature changes will take place over decadal timescales. However, dynamical changes occur on much shorter timescales (months to years). Therefore the fast-response stratospheric temperature change is the relevant quantity here.

[24] Soot heats the stratosphere strongly, which means its stratosphere-adjusted radiative forcing is 48% less than its instantaneous forcing. Therefore a larger mass of soot is required per unit radiative forcing than is indicated from calculations without stratospheric adjustment to aerosol heating. The instantaneous radiative forcing from titania is very sensitive to size, to the extent that the LARGE/WIDE distribution actually produces a weakly positive forcing ($0.04\ \mathrm{Wm}^{-2}$). It is possible that aerosol geoengineering could therefore be ineffective should our assumptions about the aerosol size distribution be incorrect. Consider a situation in the future where SRM is deployed and aerosol injected into the stratosphere, with the assumption that the aerosols will remain small. In this case we will experience a certain amount of surface cooling and certain spatial inhomogeneities governed, in part by stratospheric heating/cooling. The assumption that aerosols remain small may be incorrect, due to errors in microphysical modeling. This will change the character of both the global and regional response.

[25] The change in lower stratospheric pole-Equator temperature difference in our experiments is governed principally by the temperature change over the polar cap. Aerosols generally cool the winter pole. These results are consistent with an intensification of the polar vortex. However, in the real world the aerosol distribution will not be uniform. The layer will slope downwards towards the pole due to the sinking motion of the Brewer-Dobson circulation.

[26] We compare our results with the interannual variability in the pole-Equator temperature difference, calculated as the standard deviation of this difference in DJF and JJA over the same 20-year period as the climatology of the ES model. Monthly-mean temperature data from the NCEP-CFSR reanalysis [*Saha et al.*, 2010] are used. In DJF the inter-annual standard deviation is 2.09 K, and in JJA it is 0.64 K. In order to compare these standard deviations with our results we must multiply T_{TR-NP} by the radiative forcing. In the SMALL/WIDE case we multiply by $3.5\ \mathrm{Wm}^{-2}$. In DJF sulfate, limestone and soot increase T_{TR-NP} by more than the standard deviation in the reanalysis. In JJA sulfate increases T_{TR-NP} and soot decreases it by more than the standard deviation. Titania does not produce changes greater than the inter-annual variability in either season.

[27] Our results show significant heating perturbations in the stratosphere. This suggests that it is insufficient to model stratospheric SRM by simply reducing the total solar irradiance because this method does not capture the stratospheric aerosol heating. It is also insufficient to assume that applying the same radiative forcing with different aerosol species will have the same impact. In fact the different changes in stratospheric meridional temperature gradient will likely lead to different dynamical feedbacks and potentially produce different regional climate responses. The lower stratospheric meridional temperature gradient affects the strength of the polar vortex, which may in turn affect the Arctic Oscillation and the location of the mid-latitude storm tracks. Further dynamical modeling is required to analyse the importance of aerosol radiative absorption to the response of the stratospheric and tropospheric circulation.

[28] **Acknowledgments.** The authors would like to thank Amanda Maycock and Claire Ryder for guidance in the use of the ES code and two anonymous reviewers for their helpful comments. The CFSR data was developed by NOAA's National Centers for Environmental Prediction (NCEP).

[29] The Editor thanks two anonymous reviewers for their assistance in evaluating this paper.

References

Blackstock, J. J., et al. (2009), Climate engineering responses to climate emergencies, report, Novim, Santa Barbara, Calif.

Braesicke, P., O. Morgenstern, and J. Pyle (2010), Might dimming the sun change atmospheric ENSO teleconnections as we know them?, *Atmos. Sci. Lett.*, *12*, 184–188, doi:10.1002/asl.294.

Crutzen, P. J. (2006), Albedo enhancement by stratospheric sulfur injections: A contribution to resolve a policy dilemma?, *Clim. Change*, *77*, 211–220, doi:10.1007/s10584-006-9101-y.

Edwards, J. M., and A. Slingo (1996), Studies with a flexible new radiation code. I: Choosing a configuration for a large-scale model, *Q. J. R. Meteorol. Soc.*, *122*, 689–719, doi:10.1256/smsqj.53106.

Fels, S. B., J. D. Mahlman, M. D. Schwarzkopf, and R. W. Sinclair (1980), Stratospheric sensitivity to perturbations in ozone and carbon dioxide: Radiative and dynamical response, *J. Atmos. Sci.*, *37*, 2265–2297.

Fujii, Y. (2011), The role of atmospheric nuclear explosions on the stagnation of global warming in the mid 20th century, *J. Atmos. Sol. Terr. Phys.*, *73*, 643–652, doi:10.1016/j.jastp.2011.01.005.

Gerber, E. P., et al. (2010), Stratosphere-troposphere coupling and annular mode variability in chemistry-climate models, *J. Geophys. Res.*, *115*, D00M06, doi:10.1029/2009JD013770.

Hansen, J., M. Sato, and R. Ruedy (1997), Radiative forcing and climate response, *J. Geophys. Res.*, *102*, 6831–6864, doi:10.1029/96JD03436.

Heckendorn, P., et al. (2009), The impact of geoengineering aerosols on stratospheric temperature and ozone, *Environ. Res. Lett.*, *4*, 045108, doi:10.1088/1748-9326/4/4/045108.

Hommel, R., and H.-F. Graf (2010), Modelling the size distribution of geoengineered stratospheric aerosols, *Atmos. Sci. Lett.*, *12*, 168–175, doi:10.1002/asl.285.

Linke, C., et al. (2006), Optical properties and mineralogical composition of different Saharan mineral dust samples: A laboratory study, *Atmos. Chem. Phys.*, *6*, 2897–2922, doi:10.5194/acpd-6-2897-2006.

Maycock, A. C., K. P. Shine, and M. M. Joshi (2011), The temperature response to stratospheric water vapour changes, *Q. J. R. Meteorol. Soc.*, *137*, 1070–1082, doi:10.1002/qj.822.

Niemeier, U., H. Schmidt, and C. Timmreck (2010), The dependency of geoengineered sulfate aerosol on the emission strategy, *Atmos. Sci. Lett.*, *12*, 189–194, doi:10.1002/asl.304.

Orofino, V., A. Blanco, S. Fonti, A. C. Marra, and N. Polimeno (2002), The complex refractive index of limestone particles: An extension to the FIR range for Mars applications, *Planet. Space Sci.*, *50*, 839–847, doi:10.1016/S0032-0633(02)00058-2.

Pope, F. D., et al. (2011), Impact of geoengineered aerosols on stratospheric ozone chemistry, paper presented at European Aerosol Conference, Eur. Aerosol Assem., Manchester, U. K., 4–9 Sept.

Pueschel, R. F. (1996), Stratospheric aerosols: Formation, properties, effects, *J. Aerosol Sci.*, *27*, 383–402, doi:10.1016/0021-8502(95)00557-9.

Ramachandran, S., V. Ramaswamy, G. L. Stenchikov, and A. Robock (2000), Radiative impact of the Mount Pinatubo volcanic eruption: Lower stratospheric response, *J. Geophys. Res.*, *105*, 24,409–24,429.

Rasch, P. J., et al. (2008), An overview of geoengineering of climate using stratospheric sulphate aerosols, *Philos. Trans. R. Soc. A*, *366*, 4007–4037, doi:10.1098/rsta.2008.0131.

Ribarsky, M. W. (1985), Titanium dioxide, in *Handbook of Optical Constants of Solids*, edited by E. Palik, pp. 795–804, Academic, Orlando, Fla.

Robock, A., L. Oman, and G. L. Stenchikov (2008), Regional climate responses to geoengineering with tropical and Arctic SO_2 injections, *J. Geophys. Res.*, *113*, D16101, doi:10.1029/2008JD010050.

Robock, A., A. Marquardt, B. Kravitz, and G. Stenchikov (2009), Benefits, risks, and costs of stratospheric geoengineering, *Geophys. Res. Lett.*, *36*, L19703, doi:10.1029/2009GL039209.

Rose, D., et al. (2006), Atmospheric number size distributions of soot particles and estimation of emission factors, *Atmos. Chem. Phys.*, *6*, 1021–1031, doi:10.5194/acp-6-1021-2006.

Saha, S., et al. (2010), The NCEP Climate Forecast System Reanalysis, *Bull. Am. Meteorol. Soc.*, *91*, 1015–1057, doi:10.1175/2010BAMS3001.1.

Shepherd, J., et al. (2009), Geoengineering the climate: Science, governance and uncertainty, report, R. Soc., London.

Stenchikov, G., A. Robock, V. Ramaswamy, M. D. Schwarzkopf, K. Hamilton, and S. Ramachandran (2002), Arctic Oscillation response to the 1991 Mount Pinatubo eruption: Effects of volcanic aerosols and ozone depletion, *J. Geophys. Res.*, *107*(D24), 4803, doi:10.1029/2002JD002090.

Tegen, I., and A. A. Lacis (1996), Modeling of particle size distribution and its influence on the radiative properties of mineral dust aerosol, *J. Geophys. Res.*, *101*, 19,237–19,244, doi:10.1029/95JD03610.

Tilmes, S., R. R. Garcia, D. E. Kinnison, A. Gettelman, and P. J. Rasch (2009), Impact of geoengineered aerosols on the troposphere and stratosphere, *J. Geophys. Res.*, *114*, D12305, doi:10.1029/2008JD011420.

World Meteorological Organization (WMO) (1986), A preliminary cloudless standard atmosphere for radiation computation, *Rep. WCP-112, WMO/TD 24*, Geneva, Switzerland.

A. J. Charlton-Perez, A. J. Ferraro, and E. J. Highwood, Department of Meteorology, University of Reading, PO Box 243, Reading RG6 6BB, UK. (a.j.ferraro@pgr.reading.ac.uk)